Catalysis and rotation of F_1 motor: Cleavage of ATP at the catalytic site occurs in 1 ms before 40° substep rotation

Katsuya Shimabukuro*, Ryohei Yasuda†, Eiro Muneyuki*, Kiyotaka Y. Hara‡, Kazuhiko Kinosita, Jr.§, and Masasuke Yoshida*‡¶

*Chemical Resources Laboratory, Tokyo Institute of Technology, 4259 Nagatsuta, Midori-ku, Yokohama 226-8503, Japan; †Cold Spring Harbor Laboratory, 1 Bungtown Road, Cold Spring Harbor, NY 11724; ‡ATP System Project, Exploratory Research for Advanced Technology (ERATO), Japan Science and Technology Corporation, 5800-3, Nagatsuta, Midori-ku, Yokohama 226-0026, Japan; and §Center for Integrative Bioscience, Okazaki National Research Institute, Yamate Building 1, Higashiyama 5-138, Myodaiji, Okazaki, Aichi 444-8585, Japan

Edited by Paul D. Boyer, University of California, Los Angeles, CA, and approved October 10, 2003 (received for review August 6, 2003)

F_1, a water-soluble portion of F_oF_1-ATP synthase, is an ATP hydrolysis-driven rotary motor. The central γ-subunit rotates in the $\alpha_3\beta_3$ cylinder by repeating the following four stages of rotation: ATP-binding dwell, rapid 80° substep rotation, interim dwell, and rapid 40° substep rotation. At least two 1-ms catalytic events occur in the interim dwell, but it is still unclear which steps in the ATPase cycle, except for ATP binding, correspond to these events. To discover which steps, we analyzed rotations of F_1 subcomplex ($\alpha_3\beta_3\gamma$) from thermophilic *Bacillus* PS3 under conditions where cleavage of ATP at the catalytic site is decelerated: hydrolysis of ATP by the catalytic-site mutant F_1 and hydrolysis of a slowly hydrolyzable substrate ATPγS (adenosine 5′-[γ-thio]triphosphate) by wild-type F_1. In both cases, interim dwells were extended as expected from bulk phase kinetics, confirming that cleavage of ATP takes place during the interim dwell. Furthermore, the results of ATPγS hydrolysis by the mutant F_1 ensure that cleavage of ATP most likely corresponds to one of the two 1-ms events and not some other faster undetected event. Thus, cleavage of ATP on F_1 occurs in 1 ms during the interim dwell, and we call this interim dwell catalytic dwell.

F_oF_1-ATP synthase is an enzyme ubiquitous from bacteria to animals and plants. It synthesizes ATP from ADP and inorganic phosphate by using $\Delta\mu_H{}^+$-driven proton flow through a membrane (1, 2). F_0F_1-ATP synthase can easily be separated into two major portions: water-soluble F_1 and membrane-embedded F_o. The isolated F_1 ($\alpha_3\beta_3\gamma\delta\varepsilon$) has an ATP hydrolysis activity and is often called F_1-ATPase (3, 4). The crystal structure of F_1 shows that the rod-shaped γ-subunit is surrounded by a cylinder made of three α- and three β-subunits arranged alternatively (5). The catalytic sites are located in β-subunits but residues from adjacent α-subunits also contribute. It has been thought that F_oF_1-ATP synthase is a complex of F_o motor and F_1 motor that share a common rotor: a downhill proton flow through F_o drives rotation of the rotor, causing conformational changes in F_1 that result in ATP synthesis. Conversely, ATP hydrolysis in F_1 causes a reverse rotation of the rotor that enforces F_o to pump protons in the reverse direction (6). The rotor is made of a *c*-subunit ring of F_o (7–11) and $\gamma\varepsilon$ subunits of F_1 (12–15).

We have visualized and analyzed the ATP-driven rotation of the γ-subunit in the minimum assembly of F_1 motor, $\alpha_3\beta_3\gamma$ subcomplex (hereafter in this article, this subcomplex is called F_1) (13, 16). To date, the following features have been established. The γ-subunit makes a 120° step per one ATP consumption (17), which is further divided into 90° and 30° substeps (18). The dwelling time before the 90° substep rotation depends on ATP concentration and disappears beyond the limit of time resolution of the observation methods as ATP concentration ([ATP]) increases. Therefore, the dwell before the 90° substep rotation is a dwell for ATP binding, and the 90° substep rotation is certainly driven by ATP binding to one of β-subunits of F_1. On the contrary, dwelling time before the 30° substep rotation is independent of [ATP] and is observed even at a high [ATP] that gives a near V_{max} hydrolysis rate. Obviously, during this dwell the enzyme carries out subsequent catalytic events after ATP binding. We call the dwells before the 90° and 30° substep rotation an "ATP-binding dwell" and an "interim dwell," respectively. Histogram of the dwelling times at the 0.12-ms time resolution in the rotation assay with a probe of 40-nm bead showed that at least two events, both with a 1-ms time constant, occur in this interim dwell; the first event comes in 1 ms after ATP binding and the second event occurs in next 1 ms, which is followed by the 30° substep rotation to finish one round of catalysis (18).

Then, an immediate question is which steps in the ATPase cycle correspond to these events? Provided that the 90° substep rotation is driven by ATP binding, the subsequent steps of the ATPase reaction, namely, cleavage of ATP into ADP and P_i, release of P_i, and release of ADP, can be candidates for the two 1-ms events in the interim dwell. However, although the 90° substep rotation is clearly initiated by ATP binding, this finding does not necessarily mean that the step is driven solely by ATP binding. Taking the positive catalytic cooperativity of ATP hydrolysis by F_1 (19, 20) into account, it is possible that both ATP binding and immediately after ATP hydrolysis may drive the 90° substep rotation as proposed by Senior *et al*. (21). To address this question, we have generated two systems where the step of ATP cleavage on the enzyme is greatly decelerated. First, we have generated a catalytic-site mutant $F_{1(\beta\text{-E190D})}$, which hydrolyzes ATP extremely slowly (22). Second, we have adopted ATPγS as a slowly hydrolyzable substrate (23). The analysis of rotations under these conditions allowed us to assign one of the 1-ms events to be the cleavage of ATP at a catalytic site. In addition, the previously described "90° and 30° substeps" have been revised to the more appropriate "80° and 40° substeps."

Materials and Methods

Materials and Reagents. ATP, ADP, phospho*enol*pyruvate, and BSA were purchased from Sigma. 6-{*N*′-[2-(*N*-maleimido)-ethyl]-*N*-piperazinylamide}hexyl D-biotinamide (Biotin-PEAC$_5$-maleimide) and 1-ethyl-3-(3-dimethylaminopropyl) carbodiimide (EDC) were obtained from Dojindo (Kumamoto, Japan). Pyruvate kinase, lactate dehydrogenase, NADH, and ATPγS were acquired from Roche Diagnostics. (+)-Biotinyl-3, 6-dioxaoctanediamine (Biotin-PEO-amine) and NeutrAvidin were ob-

This paper was submitted directly (Track II) to the PNAS office.

Abbreviations: ATPγS, adenosine 5′-[γ-thio]triphosphate; fps, frames per second; rps, revolutions per second; LDAO, *N*,*N*-dimethyldodecylamine-*N*-oxide.

¶To whom correspondence should be sent at the * address. E-mail: myoshida@res.titech.ac.jp.

tained from Pierce. Carboxylate bead (diameter, 0.2 μm) was acquired from Polysciences. *N*,*N*-dimethyldodecylamine-*N*-oxide (LDAO) was obtained from Fluka.

Protein Preparation. Subcomplex ($\alpha_3\beta_3\gamma$) of F_1 from thermophilic *Bacillus* strain PS3 (called F_1 unless otherwise specified) was expressed in *Escherichia coli* JM103Δunc(uncB-D) by using an expression plasmid, pKAGB1/HC95, that carries genes for the α(C193S), γ(S107C/I210C), and β(10 His-tag at N terminus) (18). Although several residues in the expressed F_1 (called HC95) were altered from the original F_1, it functions in the same manner as the original one, and we consider HC95 as a wild type in this article. Glu-190 of β-subunit was mutated to Asp by the Kunkel method (24) with *E. coli* strain JM109 as a host. The mutant (called $F_{1(\beta\text{-E190D})}$) was expressed in JM103Δunc(uncB-D) and purified as described (25, 26). The purified F_1 was further applied to gel-filtration HPLC (Superdex 200 H/R; Amersham Biosciences) equilibrated with 100 mM KP_i, pH 7.0, containing 100 mM KCl and 2 mM EDTA, and the peak fractions were used for the experiments. The above purification procedures were carried out at room temperature. The concentration of F_1 was estimated by absorbance at 280 nm (ε = 154,000 $M^{-1}\cdot cm^{-1}$).

Hydrolysis of ATP and ATPγS. All reactions were carried out at 25°C. ATPase activity was measured in the presence of an ATP-regenerating system containing 0.2 mM NADH, 2.5 mM phospho*enol*pyruvate, 50 μg/ml pyruvate kinase, 25 μg/ml lactate dehydrogenase, and an indicated amount of ATP in solution A (50 mM KCl/2 mM $MgCl_2$/10 mM 3-[*N*-morpholino]propanesulfonic acid-KOH, pH 7.0) (27). To examine the phosphate or thiophosphate inhibitions, 0.1% LDAO was added to the assay solution to avoid effects of F_1 reactivation from the ADP-inhibited form by phosphate or thiophosphate (28). The reaction was initiated by the addition of F_1 to 1.2 ml of assay solution, and the hydrolysis rate was determined from the absorbance decrease at 340 nm. The hydrolysis rate of ATPγS was measured without an ATP-regenerating system because it replaces ATPγS with ATP during the assay. The reaction was started by mixing F_1 with indicated amount of ATPγS and stopped after various times by adding perchloric acid. The amount of produced ADP was measured by anion-exchange HPLC (10 SAX column, Whatman) eluted with 500 mM $(NH_4)_2HPO_4$-H_3PO_4, pH 4.0, monitoring absorbance at 260 nm.

Bead Preparation. Beads for rotation experiments were biotinylated as follows. The carboxylate beads (diameter, 0.2 μm) were washed twice by centrifugation with solution B (50 mM 2-morpholinoethanesulfonic acid-KOH, pH 5.5) and resuspended in solution B containing 200 μM 1-ethyl-3-(3-dimethylaminopropyl) carbodiimide and 2 mM (+)-biotinyl-3, 6-dioxaoctanediamine. After a 2-h incubation at room temperature for biotinylation, the beads were centrifuged, washed six times, suspended in solution B, and stored at 4°C.

Rotation Assay. For rotation assay, cysteines of γ-subunit were biotinylated as follows. F_1 and 6-{*N*′-[2-(*N*-maleimido)ethyl]-*N*-piperazinylamide}hexyl D-biotinamide were reacted at a molar ratio of 1:3 overnight at room temperature, and unreacted biotin was removed by PD-10 column (Amersham Biosciences). A flow chamber was made of a cover glass and a slide glass with a spacer of 50-μm thickness. Biotinylated F_1 (0.2–0.5 μM) in solution A containing 10 mg/ml BSA was loaded into the flow chamber first, and, after 2 min, F_1 unattached to the glass surface was washed away with 100 μl of solution A. Then, 2 μM NeutrAvidin in solution A was loaded. After 2 min, unbound NeutrAvidin was removed with 100 μl of solution A, and 2 pM biotinylated beads in solution A containing 10 mg/ml BSA were loaded. After a 12-min incubation, unbound beads were removed with 100 μl of solution A containing indicated amount of ATP or ATPγS. In the case of ATP, solution A was complemented by an ATP-regenerating system. Rotating duplex beads were observed with dark-field microscopy (IX-70; Olympus, Tokyo) with a ×100 objective lens (numerical aperture, 1.35; Olympus). The images of rotating beads were recorded directly to a hard disk of a computer as an 8-bit .avi file with a fast-framing charge-coupled device camera (Hi-Dcam; nac Image Technology, Tokyo) at the indicated frame rate. Custom software (created by R.Y.) was used for analyses of the bead movements and dwelling times of steps. With this experimental setup, the wild-type F_1 rotated at a rate of 24.6 ± 2.6 revolutions per second (rps) (mean ± SE; n = 5) at 2 mM ATP, far below the rate observed by the 8,000-frames per second (fps) charge-coupled device camera with 40-nm bead (≈130 rps) where viscous load did not impede the rotation (18). Therefore, the 2-ms interim dwell observed in the previous study was not seen. Nonetheless, this setup is good for observation of rotations slower than ≈10 rps because it allows long-time data collection and is easy to handle.

Results and Discussion

Bulk Phase Enzymatic Properties of $F_{1(\beta\text{-E190D})}$. To obtain a mutant F_1 in which a chemical cleavage of ATP at the catalytic site is greatly decelerated while other catalytic steps are less affected, we replaced Glu-190 of β-subunit with Asp, and $F_{1(\beta\text{-E190D})}$ was generated. Glu-190 was suggested to be an essential residue for catalysis of F_1 (29), and, indeed, the mutant $F_{1(\beta\text{-E190Q})}$ with the replacement of this critical Glu with Gln has lost ATPase activity completely (22, 30). Crystal structure of mitochondrial F_1 suggests that the carboxyl group of Glu-188 of the β-subunit (equivalent to Glu-190 of β-subunit of thermophilic F_1) acts as a general base to polarize a water molecule to make nucleophilic attack on the γ-phosphorus of ATP (Fig. 1*A*). Crystal structure also shows that βGlu-188 of mitochondrial F_1 does not directly contribute to binding AT(D)P to the catalytic site. Indeed, it was shown that a mutant *E. coli* F_1 equivalent to $F_{1(\beta\text{-E190Q})}$ had binding affinities to ATP and ADP similar to those of the wild-type F_1 (31). The $F_{1(\beta\text{-E190D})}$, as expected, retained only very low ATP hydrolytic activity. Hydrolysis of substoichiometric amount of ATP (unisite catalysis) by $F_{1(\beta\text{-E190D})}$ (time constant, 126 s) was 1,800 times as slow as the wild-type F_1 (time constant, 6.9×10^{-2} s) (32). Steady-state ATPase activity of $F_{1(\beta\text{-E190D})}$ showed simple Michaelis–Menten-type dependence on [ATP], and the V_{max} and K_m values (mean ± SE) were determined to be 2.4 ± 0.0 s^{-1} and 1.4 ± 0.1 μM, respectively (Fig. 1*B*). This V_{max} value is ≈100 times smaller than that of the wild-type F_1 (≈250 s^{-1}). This K_m value is one order smaller than that of the wild-type F_1 (19 ± 1 μM) measured in the presence of LDAO, a suppressor of the MgADP inhibition (18).

Rotation of $F_{1(\beta\text{-E190D})}$. We observed rotation of $F_{1(\beta\text{-E190D})}$ at various [ATP]s. At all [ATP]s, the rotation rate averaged over 30 s roughly agreed with the ATP hydrolysis rate measured in the bulk divided by 3 (Fig. 1*B*). Some 20% of the higher rate of the rotation than ATP hydrolysis can be explained by MgADP inhibition in the latter condition. In bulk phase kinetics, some fraction of enzyme is always in the state of MgADP inhibition. On the other hand, rotation rate was measured for only actively rotating molecules and hardly was affected by MgADP inhibition. A rotation vs. [ATP] curve could be fitted with a simple Michaelis–Menten-type kinetics, where V_{max} and K_m values (mean ± SE) were calculated to be 0.9 ± 0.1 rps (for 2.7 s^{-1} ATP hydrolysis) and 1.0 ± 0.4 μM, respectively. Unlike the wild-type F_1, $F_{1(\beta\text{-E190D})}$ rotated with discrete 120° steps even at 2 mM ATP (Fig. 2*A*). As will be discussed later, these dwells are not the ATP-binding dwells but the interim dwells. At low [ATP] (<2 μM), the 120° steps were further divided into two substeps, and

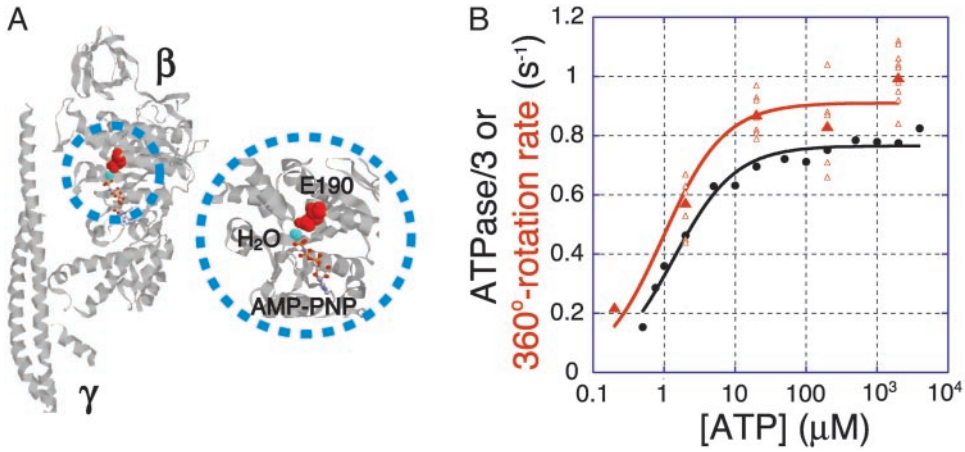

Fig. 1. (*A*) The position of Glu-190 of β-subunit. The structural data are taken from chain F of bovine mitochondrial F_1-ATPase (Protein Data Bank ID code 1BMF; ref. 5). β-Subunit and γ-subunit are shown as ribbon models (*Left*). Residue Glu-188 (red), equivalent to Glu-190 in this study, and a water (cyan), which is thought to be important for catalysis, are shown as space-filling models. 5′-(β,γ-Imino)triphosphate (AMP-PNP), an analogue of ATP, is shown as a stick model. Close-ups of the regions near Glu-188 and AMP-PNP are shown (*Right*). (*B*) Comparison of the 360° rotation rate and hydrolysis rates in the bulk. Black circle, the rate of the ATP hydrolysis in the bulk divided by 3; red open triangle, averaged 360° rotation rate for the individual 0.2-μm duplex beads attached to γ-subunit of $F_{1(\beta\text{-E190D})}$; red filled triangle, the 360° rotation rate averaged over different beads. The black and red lines show fit with Michaelis–Menten equation, $V = V_{max} \times [ATP]/(K_m + [ATP])$. $V_{max} = 0.8 \pm 0.0\ s^{-1}$ and $K_m = 1.4 \pm 0.1\ \mu M$ for the bulk, $V_{max} = 0.9 \pm 0.1\ s^{-1}$ and $K_m = 1.0 \pm 0.4\ \mu M$ for rotation. Values are means ± SE.

the steps at six regular positions were observed in one revolution (Fig. 2*B* and *Inset*). The angles of the two substep rotations were ≈80° (80.9 ± 1.8°; mean ± SE; $n = 15$) and ≈40° (39.1 ± 1.7°). The dwelling time before the 80° substep rotation depended on [ATP], therefore, this dwell is the ATP-binding dwell. On the other hand, the dwelling time before the 40° substep rotation was independent of [ATP], and this dwell is the interim dwell.

The 80° and 40° substeps described here correspond to the previously reported 90° and 30° substeps (18). The apparent discrepancy in the angles seems to arise from the difference between the observation methods. In the previous study, a 40-nm single bead obliquely attached to the γ-subunit was used as a probe of rotation, whereas we used 0.2-μm duplex beads in the present study. With a larger probe, better angular resolution was attained in the present study. The study on MgADP inhibition also presented 37.6 ± 2.5° as an angle of substep rotation that precedes the ATP-binding dwell (33). Therefore, although the very accurate angles of substep rotations should be determined in future studies, the terms 80° and 40° substeps are more appropriate at present than the previous 90° and 30° substeps.

Dwelling Times of Rotation of $F_{1(\beta\text{-E190D})}$. Histogram of the ATP-binding dwell before 80° substeps obeyed an exponential function (data not shown), and the second-order rate constant for ATP binding to F_1 (k_{on}) was estimated to be $(3.1 \pm 0.1) \times 10^6\ M^{-1}\cdot s^{-1}$ (mean ± SE). This k_{on} value of $F_{1(\beta\text{-E190D})}$ is approximately one order smaller than that of the wild-type [$(3.0 \pm 0.1) \times 10^7\ M^{-1}\cdot s^{-1}$) (18), probably because of the subtle change of environments near γ-phosphate of ATP caused by replacing Glu with Asp. If we apply a simple Michaelis–Menten scheme,‖ the 10-fold decrease in K_m is consistent with the observed 10-fold decrease in k_{on} and 100-fold decrease in k_{cat} on the assumption that k_{off} is negligible compared with k_{cat}. Histogram of the interim dwell has a distinct peak, which can be fit with double exponentials with two time constants of 321 ± 22 ms and 19.9 ± 0.1 ms (mean ± SE) (Fig. 2*C*). Thus, the interim dwell of $F_{1(\beta\text{-E190D})}$ is comprised of at least two kinds of successive dwells: a relatively long dwell of 320 ms and a relatively short dwell of 20 ms. Considering the properties of the mutant described above, it is most likely that the longer dwell corresponds to the time required for the chemical cleavage of ATP.

Hydrolysis of ATPγS by F_1. ATPγS often has been regarded as a nonhydrolyzable ATP analogue and used as an inhibitor of phosphatases and ATPases. However, when ATPγS was incubated with F_1, the amount of ATPγS was slowly decreased (Fig. 3*A Inset*) and an equivalent amount of ADP was produced (not shown). Without F_1, no such change occurred. Thus, ATPγS is a slowly hydrolyzable substrate for F_1-ATPase. The hydrolysis rate of ATPγS did not show simple Michaelis–Menten dependence on ATPγS concentration ([ATPγS]) and could be fitted with an equation assuming two K_m values (27). The total V_{max} value of ATPγS hydrolysis by the wild-type F_1 was $5.8 \pm 0.3\ s^{-1}$ (mean ± SE), and this value is 43 times smaller than that of ATP hydrolysis (≈$250\ s^{-1}$). The K_m values are 1.0 ± 0.3 μM and (2.4 ± 1.0) × 10^2 μM (Fig. 3*A*). The higher K_m value of several hundred micromolar also was observed during ATP hydrolysis by wild-type F_1 in the absence of LDAO, and it was concluded as representing MgATP binding to noncatalytic sites, which reactivates the MgADP-inhibited enzyme (34–36). Similarly, we regard the high K_m value of (2.4 ± 1.0) × 10^2 μM observed for ATPγS as also reflecting MgATPγS binding to noncatalytic sites. The reason for the slow hydrolysis of ATPγS is mainly the sluggish cleavage of ATPγS on the catalytic site. Actually, the binding property of ATPγS to the catalytic site is not so different from ATP as examined by rapid mixing experiments (32). If the release of thiophosphate, one of the hydrolyzed products of ATPγS, from the catalytic site were extremely slow, it would cause the decrease of V_{max} value. However, it does not seem to be the case, because even in the presence of 100 mM thiophosphate, the ATPase activity was decreased by only 57% (Fig. 3*B*). This inhibition, although a little greater than that exhibited by P_i, which decreased by 51% at 100 mM, cannot explain the extent of decrease in V_{max} value of ATPγS hydrolysis.

Rotation of F_1 by ATPγS. The rotation rate at 20 μM ATPγS (5.9 rps; mean; $n = 2$) was similar to the rate at 2 mM ATPγS (4.4 ± 0.3 rps; mean ± SE; $n = 5$), and discrete 120° steps were observed (Fig. 4*A*). The hydrolysis rate estimated from rotation assay was

‖Here we assume that K_m is expressed as $(k_{off} + k_{cat})/k_{on}$, where k_{on} is a second-order ATP-binding rate constant, k_{off} is an ATP-release rate constant, and k_{cat} is a rate constant to produce products from enzyme-substrate complex.

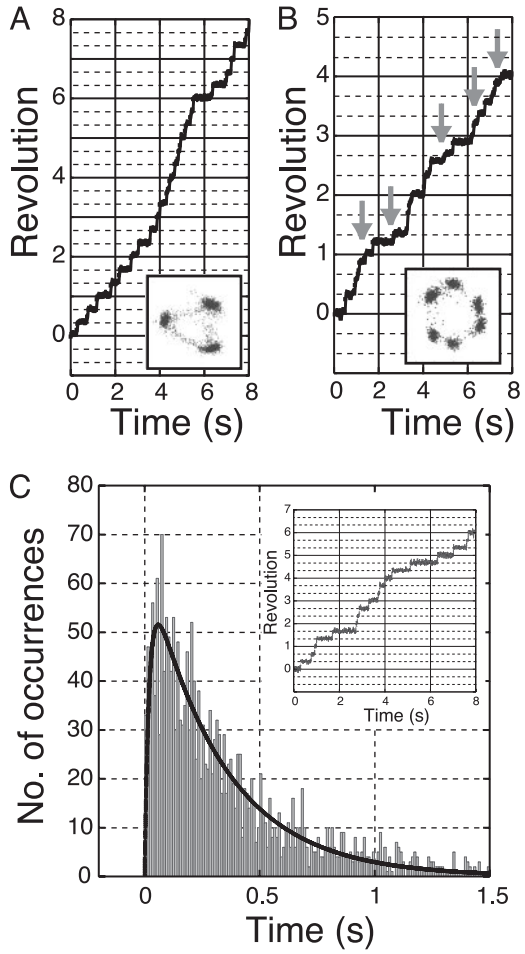

Fig. 2. (*A* and *B*) Typical time course of the stepwise rotations of $F_{1(\beta\text{-E190D})}$ at 2 mM (*A*) and 2 μM (*B*) ATP at 30 fps. (*Insets*) The trace of the centroid of the beads images. Arrows indicate the positions at which 40° substep was observed. (*C*) The histogram of dwelling times between steps in the presence of 2 mM ATP at 500 fps. Total counts are 2,068. (*Inset*) The time course of rotation at 500 fps. Black line shows fit with two exponentials assuming there were two rate-limiting reactions: constant $\times$ (exp($-k_1 \times t$) $-$exp($-k_2 \times t$)), where k_1 = 50.3 $\pm$ 0.2 s^{-1} (mean $\pm$ SE; time constant, 19.9 $\pm$ 0.1 ms) and k_2 = 3.12 $\pm$ 0.22 s^{-1} (time constant, 321 $\pm$ 22 ms).

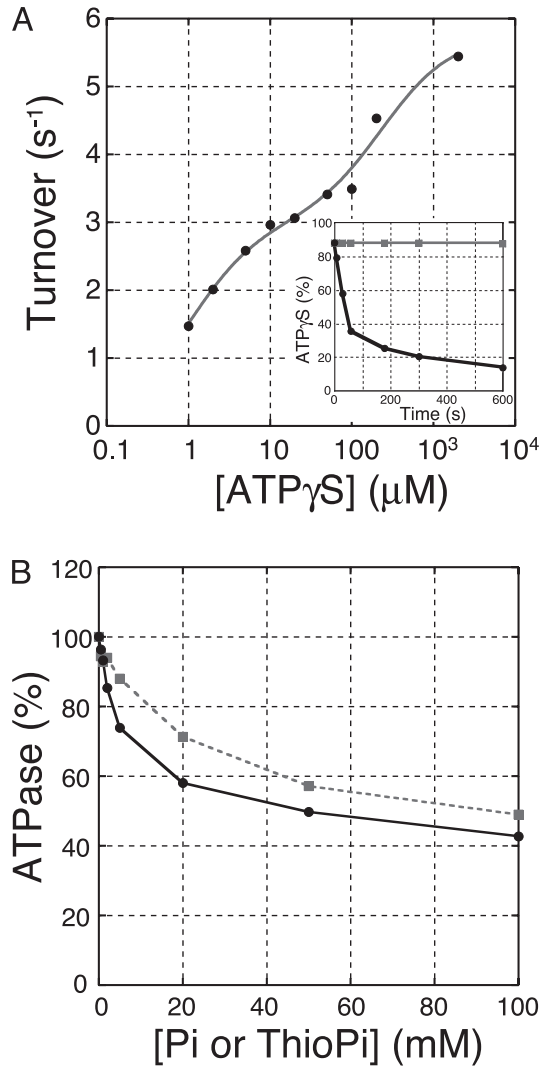

Fig. 3. (*A*) ATPγS hydrolysis rate as a function of ATPγS concentration. The solid curve is the fit with two K_m values: $V = (V_{max1} \times K_{m2} \times [ATP] + V_{max2} \times [ATP]^2)/([ATP]^2 + K_{m2} \times [ATP] + K_{m1} \times K_{m2})$, where V_{max1} = 3.0 $\pm$ 0.2 s^{-1}, V_{max2} = 5.8 $\pm$ 0.3 s^{-1}, K_{m1} = 1.0 $\pm$ 0.3 μM, and $K_{m2} = (2.4 \pm 1.0) \times 10^2$ μM. (*Inset*) The time courses of ATPγS hydrolysis. Black circles, in the presence of 200 μM ATPγS and 0.5 μM F_1 (wild type); gray squares, in the absence of F_1. (*B*) The rate of ATP hydrolysis in the presence of phosphate (gray squares) or thiophosphate (black circles). Values are means $\pm$ SE.

twice as high as that measured in the bulk solution, presumably because some of the F_1 molecules in the solution were in the MgADP-inhibited form. The difference was greater than in the case of ATP because we could not use an ATP-regenerating system for ATPγS. The dwells between the steps are independent of [ATPγS], indicating that they are the interim dwells. This finding also excluded a possibility that rotation was driven by contaminated ATP that was <0.1%, as assessed with an anion-exchange HPLC. At 0.5 μM ATPγS,** rotations with 80° and 40° substeps were observed (Fig. 4*B*). From analysis of ATPγS-binding dwells, the second-order rate constant for ATPγS binding to F_1 (k_{on}) was estimated to be $(2.6 \pm 0.1) \times 10^7$ $M^{-1}{\cdot}s^{-1}$ (mean $\pm$ SE), which is similar to that of ATP [$(3.0 \pm 0.1) \times 10^7$ $M^{-1}{\cdot}s^{-1}$] (18) and agrees well with the value determined from a biochemical experiment [$(2.8 \pm 0.2) \times 10^7$ $M^{-1}{\cdot}s^{-1}$] (32). Histogram of the interim dwells showed an upward convex shape passing through the origin (Fig. 4*C*), which can be fit by double exponentials with two time constants of 61.0 $\pm$ 2.6 ms and 8.20 $\pm$ 0.6 ms (mean $\pm$ SE). Biochemical studies suggest that ATPγS decelerates the cleavage rate by 30-fold (23). Thus, the longer dwell most likely corresponds to the slow cleavage of ATPγS and the short one corresponds to the product release, as discussed later.

Rotation of $F_{1(\beta\text{-E190D})}$ by ATPγS. We assume that both the 320-ms event of $F_{1(\beta\text{-E190D})}$ in hydrolysis of ATP and the 61-ms event of F_1 in hydrolysis of ATPγS correspond to the same rate-limiting reaction, that is, cleavage of terminal (thio)phosphate moiety of ATP or ATPγS. To further confirm this point, we analyzed the rotation of $F_{1(\beta\text{-E190D})}$ driven by the hydrolysis of ATPγS. At 2 mM ATPγS, very slow rotation ($2.3 \times 10^{-2} \pm 0.3$ rps; mean $\pm$ SE; n = 5) was observed, and rotation proceeded with discrete 120° steps (Fig. 5*A*). Histogram of the dwelling times showed an apparent single-exponential decay, and a value of 12.5 $\pm$ 0.4 s

**At low ATPγS concentrations (<2 μM), rotating beads were rarely seen in the observation field, probably because of the MgADP inhibition. Usually the ATP-regenerating system eliminates ADP, but it cannot be used in these experiments because it replaces ATPγS with ATP.

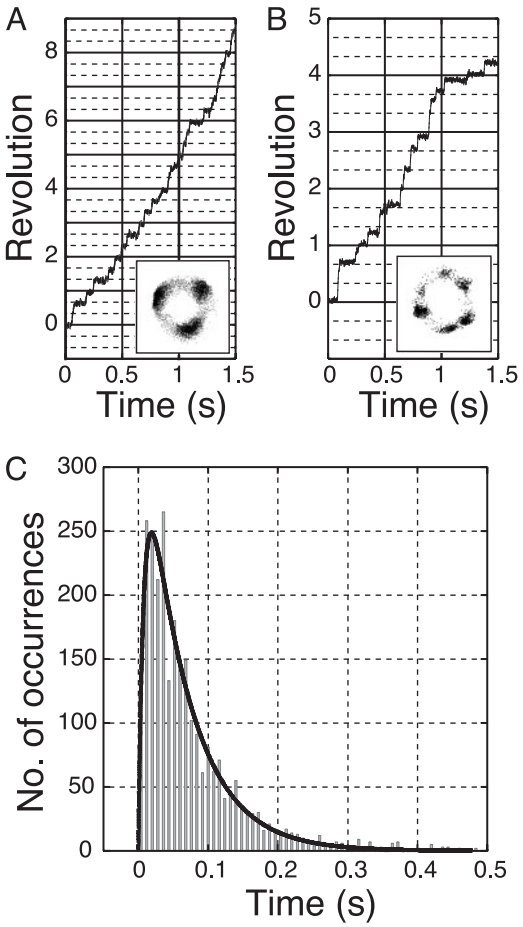

Fig. 4. (*A* and *B*) Typical time course of the rotation of 0.2-μm duplex beads attached to γ-subunit of F_1 (wild type) with 2 mM (*A*) and 0.5 μM (*B*) ATPγS at 500 fps. (*Insets*) The trace of the centroid of the bead images. (*C*) The histogram of the dwelling times between steps at 2 mM ATPγS by using a fast-framing camera at 500 fps (2,674 dwells). Black line shows fit with two exponentials as in Fig. 2*C*: $k_1 = (1.22 \pm 0.09) \times 10^2\ s^{-1}$ (mean $\pm$ SE; time constant, 8.20 $\pm$ 0.6 ms) and $k_2 = 16.4 \pm 0.7\ s^{-1}$ (time constant, 61.0 $\pm$ 2.6 ms).

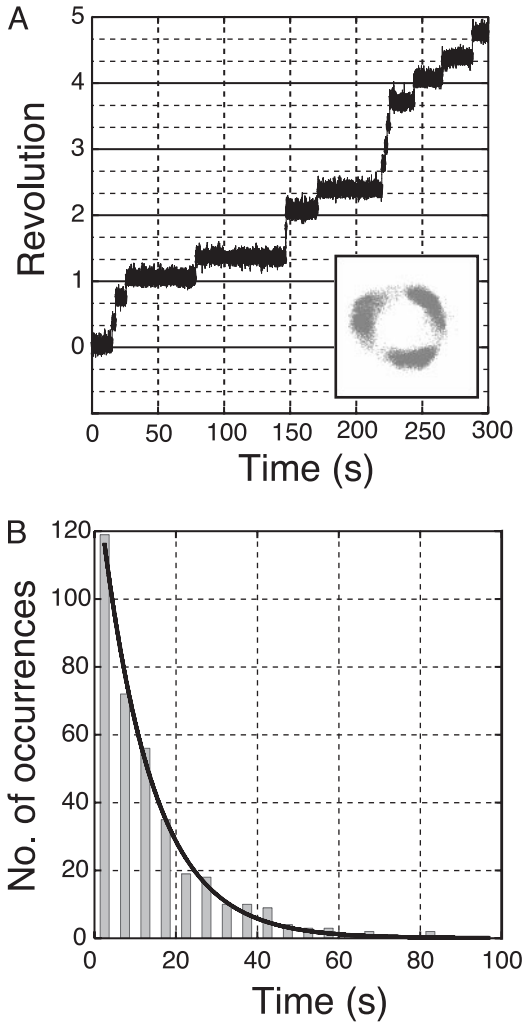

Fig. 5. (*A*) Time course of the stepwise rotation of $F_{1(\beta\text{-E190D})}$ in the presence of 2 mM ATPγS at 250 fps. (*Inset*) The trace of the centroid of 0.2-μm beads. (*B*) The histogram of dwelling times between steps in the presence of 2 mM ATPγS at 250 fps (363 dwells). Black line shows a single exponential fit: constant $\times$ exp($-k \times t$), where k is the rate constant and t is the dwelling time; $k = (8.00 \pm 0.27) \times 10^{-2}\cdot s^{-1}$ (mean $\pm$ SE; time constant, 12.5 $\pm$ 0.4 s)

(mean $\pm$ SE) was obtained as the time constant[††] (Fig. 5*B*). The very long time constant observed in the combination of the mutation and ATPγS is consistent with the contention that the main effect of βE190D mutation and ATPγS is to retard the same step of ATP(γS) cleavage. Furthermore, if we assume that their effects are energetically additive, the very long time constant leads a conclusion that one of the two 1-ms events in the interim dwell of the wild-type F_1 is the cleavage of ATP. Actually, if we assume that one of the two 1-ms events in the interim dwell of the wild-type F_1 is the cleavage of ATP at the catalytic site, the mutation βE190D and ATPγS slowed down the time constant of this event 320-fold and 61-fold, respectively. Then, if modification of a catalytic residue and a substrate might exhibit a dual effect on the catalytic rate (rotation rate), the time constant of ATPγS cleavage by $F_{1(\beta\text{-E190D})}$ is predicted to be 19.5 s (for 1 ms $\times$ 320 $\times$ 61). The value obtained from the experiment, 12.5 s, is fairly close to this predicted value and strongly suggests that these assumptions are valid. This agreement also exclude the possibility that a third, unidentified event with a faster time constant corresponds to the ATP cleavage. For example, if an event of 0.1 ms corresponded to the ATP cleavage at the catalytic site, the mutation βE190D and ATPγS would retard the step by 3,200-fold and 610-fold, respectively. Then, the combination of the mutant and ATPγS would cause 1,952,000-fold deceleration, resulting in a time constant as long as 195.2 s. This value is far larger than the experimental value observed, and the above possibility is proved to be unlikely. Thus, cleavage of ATP on F_1 occurs in 1 ms during the interim dwell, and we call this interim dwell the catalytic dwell. The present results also indicate that the 80° substep rotation takes place before the cleavage of ATP into ADP and P_i and the 40° substep rotation requires completion of the cleavage.

Conclusion

In the function of F_1, catalysis and rotation seems to be tightly coupled. Therefore, altered catalysis, either by mutation or different substrate, results in altered rotation, and analysis of the latter with good reference of the former can bring a insight into the mechanism of F_1 motor. We have adopted this approach and obtained results leading to the conclusion that the ATP cleavage reaction at the catalytic site is one of the 1-ms events in the

[††]A short dwell with a time constant $<$0.2 s might exist but could not be seen in the present observations.

catalytic dwell. Contrary to the previous hypothesis (21), it is clearly indicated that the 80° substep rotation takes place before the cleavage of ATP into ADP and P_i. It also is established that the 40° substep rotation requires completion of the cleavage. This conclusion was to be expected but needed to be examined experimentally because the two 1-ms events can be any events (except ATP binding) that occur in F_1 during catalysis. Even a conformational isomerization of F_1 without changes of chemical species of bound substrate/product cannot be excluded as a candidate. Now that one of the 1-ms events is determined to be an ATP cleavage, the next challenge will be the identification of another 1-ms event and clarification of the sequence of the events.[‡‡]

[‡‡]If the two catalytic events occur at the same β-subunit, ATP hydrolysis must occur first followed by release of products. But in the case where the two events occur at different β-subunits, ATP hydrolysis could occur after product release from another β-subunit.

We thank H. Noji, R. Iino, T. Masaike, Y. Hirono-Hara, T. Ariga, H. Ueno, T. Suzuki, and M. Takeda for critical discussions and technical advice. K.S. is supported by research fellowships from the Japan Society for the Promotion of Science for Young Scientists.

1. Mitchell, P. (1961) *Nature* **191,** 144–148.
2. Boyer, P. D. (2000) *Biochim. Biophys. Acta* **1458,** 252–262.
3. Yoshida, M., Muneyuki, E. & Hisabori, T. (2001) *Nat. Rev. Mol. Cell. Biol.* **2,** 669–677.
4. Noji, H. & Yoshida, M. (2001) *J. Biol. Chem.* **276,** 1665–1668.
5. Abrahams, J. P., Leslie, A. G., Lutter, R. & Walker, J. E. (1994) *Nature* **370,** 621–628.
6. Boyer, P. D. (1993) *Biochim. Biophys. Acta* **1140,** 215–250.
7. Kaim, G. & Dimroth, P. (1998) *EMBO J.* **17,** 5887–5895.
8. Sambongi, Y., Iko, Y., Tanabe, M., Omote, H., Iwamoto-Kihara, A., Ueda, I., Yanagida, T., Wada, Y. & Futai, M. (1999) *Science* **286,** 1722–1724.
9. Hutcheon, M. L., Duncan, T. M., Ngai, H. & Cross, R. L. (2001) *Proc. Natl. Acad. Sci. USA* **98,** 8519–8524.
10. Nishio, K., Iwamoto-Kihara, A., Yamamoto, A., Wada, Y. & Futai, M. (2002) *Proc. Natl. Acad. Sci. USA* **99,** 13448–13452.
11. Tsunoda, S. P., Aggeler, R., Yoshida, M. & Capaldi, R. A. (2001) *Proc. Natl. Acad. Sci. USA* **98,** 898–902.
12. Sabbert, D., Engelbrecht, S. & Junge, W. (1996) *Nature* **381,** 623–625.
13. Noji, H., Yasuda, R., Yoshida, M. & Kinosita, K., Jr. (1997) *Nature* **386,** 299–302.
14. Kato-Yamada, Y., Noji, H., Yasuda, R., Kinosita, K., Jr., & Yoshida, M. (1998) *J. Biol. Chem.* **273,** 19375–19377.
15. Omote, H., Sambonmatsu, N., Saito, K., Sambongi, Y., Iwamoto-Kihara, A., Yanagida, T., Wada, Y. & Futai, M. (1999) *Proc. Natl. Acad. Sci. USA* **96,** 7780–7784.
16. Adachi, K., Yasuda, R., Noji, H., Itoh, H., Harada, Y., Yoshida, M. & Kinosita, K., Jr. (2000) *Proc. Natl. Acad. Sci. USA* **97,** 7243–7247.
17. Yasuda, R., Noji, H., Kinosita, K., Jr., & Yoshida, M. (1998) *Cell* **93,** 1117–1124.
18. Yasuda, R., Noji, H., Yoshida, M., Kinosita, K., Jr., & Itoh, H. (2001) *Nature* **410,** 898–904.
19. Cross, R. L., Grubmeyer, C. & Penefsky, H. S. (1982) *J. Biol. Chem.* **257,** 12101–12105.
20. Grubmeyer, C., Cross, R. L. & Penefsky, H. S. (1982) *J. Biol. Chem.* **257,** 12092–12100.
21. Senior, A. E., Nadanaciva, S. & Weber, J. (2002) *Biochim. Biophys. Acta* **1553,** 188–211.
22. Amano, T., Tozawa, K., Yoshida, M. & Murakami, H. (1994) *FEBS Lett.* **348,** 93–98.
23. Turina, P. & Capaldi, R. A. (1994) *Biochemistry* **33,** 14275–14280.
24. Kunkel, T. A., Bebenek, K. & McClary, J. (1991) *Methods Enzymol.* **204,** 125–139.
25. Amano, T., Hisabori, T., Muneyuki, E. & Yoshida, M. (1996) *J. Biol. Chem.* **271,** 18128–18133.
26. Matsui, T. & Yoshida, M. (1995) *Biochim. Biophys. Acta* **1231,** 139–146.
27. Kato, Y., Sasayama, T., Muneyuki, E. & Yoshida, M. (1995) *Biochim. Biophys. Acta* **1231,** 275–281.
28. Mitome, N., Ono, S., Suzuki, T., Shimabukuro, K., Muneyuki, E. & Yoshida, M. (2002) *Eur. J. Biochem.* **269,** 53–60.
29. Yoshida, M., Posper, J. W., Allison, W. S. & Esch, F. S. (1981) *J. Biol. Chem.* **256,** 148–153.
30. Ohtsubo, M., Yoshida, M., Ohta, S., Kagawa, Y., Yohda, M. & Date, T. (1987) *Biochem. Biophys. Res. Commun.* **146,** 705–710.
31. Lobau, S., Weber, J., Wilke-Mounts, S. & Senior, A. E. (1997) *J. Biol. Chem.* **272,** 3648–3656.
32. Masaike, T., Muneyuki, E., Noji, H., Kinosita, K., Jr., & Yoshida, M. (2002) *J. Biol. Chem.* **277,** 21643–21649.
33. Hirono-Hara, Y., Noji, H., Nishiura, M., Muneyuki, E., Hara, Y. K., Yasuda, Y., Kinosita, K., Jr., & Yoshida, M. (2001) *Proc. Natl. Acad. Sci. USA* **98,** 13649–13654.
34. Jault, J. M. & Allison, W. S. (1993) *J. Biol. Chem.* **268,** 1558–1566.
35. Ren, H. & Allison, W. S. (2000) *J. Biol. Chem.* **275,** 10057–10063.
36. Ono, S., Hara, Y. K., Hirao, T., Matsu, T., Noji, H., Yoshida, M. & Muneyuki, E. (2003) *Biochim. Biophys. Acta.* **1607,** 35–44.